Chemical Engineering Journal 159 (2010) 129–137

Contents lists available at ScienceDirect

Chemical Engineering Journal

journal homepage: www.elsevier.com/locate/cej

Enhanced catalytic activity and stability of $Cu_{0.13}Ce_{0.87}O_y$ catalyst for acetone combustion: Effect of calcination temperature

Chaoquan Hu[a,b,*]

[a] State Key Laboratory of Multiphase Complex System, Institute of Process Engineering, Chinese Academy of Sciences, Beijing 100190, China
[b] Institute of Engineering Thermophysics, Chinese Academy of Sciences, Beijing 100190, China

ARTICLE INFO

Article history:
Received 7 September 2009
Received in revised form 1 March 2010
Accepted 2 March 2010

Keywords:
Nanocrystalline
$Cu_{0.13}Ce_{0.87}O_y$
Volatile organic compound
Catalytic combustion
Stability

ABSTRACT

The aim of this work was to improve the catalytic activity and stability of $Cu_{0.13}Ce_{0.87}O_y$ catalyst for acetone combustion by varying the preparation route. Nanocrystalline $Cu_{0.13}Ce_{0.87}O_y$ catalyst was prepared by a co-precipitation method combined with a supercritical drying technique and calcination steps. The effect of calcination temperature on the structural feature and the catalytic behavior of the $Cu_{0.13}Ce_{0.87}O_y$ catalyst was examined in order to obtain the best catalytic performance and identify any factor that may be favorable for acetone combustion. The structural characteristics of the catalysts calcined at different temperatures were investigated in detail by X-ray diffraction (XRD), scanning electron microscopy (SEM), Raman spectroscopy, X-ray photoelectron spectroscopy (XPS), and temperature-programmed reduction (TPR) techniques. The experimental results revealed that the structure and catalytic performance of the as-prepared $Cu_{0.13}Ce_{0.87}O_y$ catalyst were dependent on the calcination temperature. The catalyst calcined at 700 °C exhibited the best catalytic activity for acetone combustion and could catalyze the complete combustion of acetone at a temperature as low as 200 °C with almost 100% CO_2 selectivity. The endurance tests showed that the developed catalysts calcined from 400 to 700 °C possessed good stability for acetone combustion over 50 h of continuous operation despite their different stability behaviors under the present experimental conditions.

1. Introduction

Acetone is a common organic solvent widely used in modern industrial production processes. Its emission can give rise to many environmental problems and do harmful to human health. Various end-of-pipe techniques have been developed to reduce its emission. Among them, catalytic combustion that converts it into non-toxic carbon dioxide and water has been recognized as one of the most promising techniques. The catalytic performance of the employed catalyst is one of the important factors determining the effectiveness of this technique. Generally, two types of catalysts, noble metals and transition metal oxides, are used for the catalytic combustion of acetone. Although the former usually have higher activities toward oxidation reactions [1,2], the high costs of noble metals limit their wide applications. The development of highly active and thermally stable metal oxide catalysts would be advantageous to provide a low-cost alternative to noble metals for catalytic combustion of acetone.

Up to now, transition metal oxides and their combinations, such as Co_3O_4, MnO_x, CuO and CeO_2, have been evaluated as catalysts for acetone combustion [3–10]. A favorable synergistic effect between the metal oxides is always proposed to explain their highly catalytic activities for oxidation reactions [11–13]. Our previous studies demonstrated that the $Cu_{0.13}Ce_{0.87}O_y$ catalyst prepared by a combustion method exhibited a high catalytic activity for acetone combustion [14]. However, the stability of the $Cu_{0.13}Ce_{0.87}O_y$ catalyst for acetone combustion was poor under the selected experimental conditions and an obvious deactivation was observed under the reactant stream for 35 h. The deactivation of the catalyst was mainly caused by the aggregation of highly dispersed copper species into bulk CuO phase, which prevented the synergistic effect between CeO_2 and CuO and thus decreased its catalytic activity for acetone combustion. Similar deactivation of CuO/CeO_2 catalyst for oxidation reaction was also observed due to the sintering of dispersed copper species on the catalyst surface [15]. Thus, the inhibition of aggregation or sintering of the dispersed copper species on the catalyst surface appears to be the key factor in improving the catalyst stability for acetone combustion.

It has been widely accepted that catalytic performance of an inorganic material catalyst is greatly related to the preparation method that always has effect on the structural characteristics of the catalyst. For mixed oxide catalysts, the interaction among oxide

* Correspondence address: Institute of Engineering Thermophysics, Chinese Academy of Sciences, Beijing 100190, China. Tel.: +86 10 82543120.
E-mail addresses: cqhu@home.ipe.ac.cn, cq_hu@hotmail.com.

1385-8947/$ – see front matter © 2010 Elsevier B.V. All rights reserved.
doi:10.1016/j.cej.2010.03.007

phases and the dispersion of active phase are always considered to be two main parameters that affect catalytic activity and stability of the catalysts [16,17]. Wang and Ruckenstein reported that the formation of CoO–MgO solid solution and a strong interaction between them were crucial to its stability for partial oxidation of methane [18]. Baylet et al. demonstrated that Pd doped hexaaluminate catalyst exhibited stable catalytic activity for methane combustion due to the high dispersion of Pd in the catalyst [19]. It seems that the stability of the $Cu_{0.13}Ce_{0.87}O_y$ catalyst for acetone combustion may be enhanced by increasing the dispersion of copper species and strengthening the interaction between CuO and CeO_2. In this case, nanoscale materials may offer significant promise due to their small crystallite sizes and high homogeneity of constituents, which would favor the formation of metal oxide solid solution and ensure a good dispersion of active phase.

In the present study, nanocrystalline $Cu_{0.13}Ce_{0.87}O_y$ catalyst was prepared by a co-precipitation method followed by a supercritical drying and calcination steps. The present method for preparation of catalyst combines the advantages of co-precipitation method, such as obtaining homogeneous mixed oxides with a good control of stoichiometry, and supercritical technique enabling maintenance of the hydrogel structure and decrease in aggregation degree of the nanocrystals. The effect of the calcination temperature on the structural feature and the catalytic performance of the catalyst was investigated in detail.

2. Experimental

2.1. Catalyst preparation

All the reagents were of analytical grade and used as received without further purification. Nanocrystalline $Cu_{0.13}Ce_{0.87}O_y$ catalyst was prepared using the raw materials of $Cu(NO_3)_2{\cdot}3H_2O$, $Ce(NO_3)_3{\cdot}6H_2O$, NaOH and polyethyleneglycol (PEG). Typically, 1.30 mmol $Cu(NO_3)_2{\cdot}3H_2O$ and 8.70 mmol $Ce(NO_3)_3{\cdot}6H_2O$ together with 5 mmol% PEG were dissolved into 1000 mL deionized water to form a solution with the total metal ion concentration of 0.01 M. A 0.01 M NaOH solution was then added dropwise to the above solution under continuously vigorous stirring at room temperature until the metal ions were completely precipitated. The pH of the final solution was 9.0 ± 0.2. The resultant hydrogel was aged for 2 h at room temperature, followed by filtering and repeatedly washing with deionized water and absolute ethanol to remove the free water involved in the hydrogel. The as-obtained gel was treated in an autoclave at the ethanol supercritical drying (SCD) condition of 260 °C and 8.0 MPa for 1 h. After the release of the ethanol vapor at 260 °C, the dried powder was cooled down to room temperature with a continuous argon flow. The resultant powder was further calcined in air at different temperatures for 4 h.

2.2. Catalyst characterizations and catalytic performance evaluation

The composition of the as-prepared $Cu_{0.13}Ce_{0.87}O_y$ sample was confirmed by inductively coupled plasma atomic emission spectroscopy (ICP-AES) on a PE OPTIMA 5300 DV spectrometer. Differential scanning calorimetric analysis (DSC) and thermogravimetric analysis (TG) were carried out on a simultaneous TG–DTA/DSC apparatus (NETZSCH STA 449C, Germany) with a heating rate of 20 °C/min in a flowing air atmosphere. The phase structure of all the samples was analyzed by an X-ray diffractometer (X'Pert MPD Pro, PANalytical, The Netherlands). The morphology was examined by field-emission scanning electron microscopy (FESEM, JSM-6700F, JEOL). N_2 adsorption/desportion isotherms of the samples were obtained at 77 K using an autosorb-1 gas system (Quantachrome Instruments, USA). The specific surface area was determined by using the linear portion of the Brunauer–Emmett–Teller (BET) model and the average pore size was calculated by using the Barret–Joyner–Halenda (BJH) formula from the desorption branch of the isotherms. Prior to the measurement, the sample was outgassed at 300 °C for 4 h. The Raman spectrum was obtained on a LabRAM HR800 spectrometer (Horiba Jobin Yvon, France) equipped with a 514 nm single-frequency laser and a CCD detector at ambient temperature and moisture-free conditions.

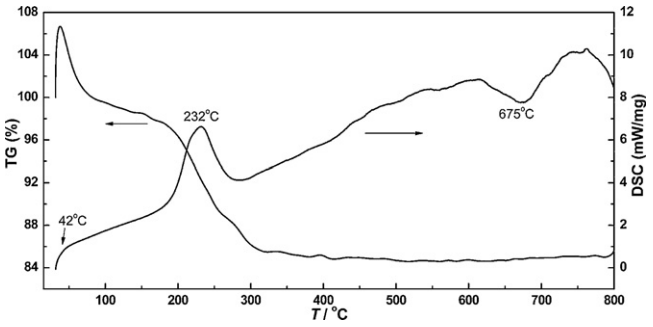

Fig. 1. TG–DSC curves of the as-prepared $Cu_{0.13}Ce_{0.87}O_y$ precursor.

The details of the other characterization techniques and the catalytic performance evaluation have been described in the previous work [14]. Briefly, acetone vapor was carried by an air stream bubbling through a boat-shaped saturator in ice-bath and diluted with another air-flow before reaching the catalyst bed that consisted of 0.2 g catalyst (20–40 mesh) and certain amounts of silica (20–40 mesh). The total flow rate was about 200 mL/min. To prevent the physisorption of acetone in the initial stages of the test, the catalyst was pretreated at 100 °C for 30 min under the test flows of reactant mixture (1000 ppm acetone balanced by dry air). When a steady state was attained, the temperature was raised stepwise per 10 °C from 100 °C to the temperature that could achieve the complete conversion of acetone. The acetone concentration in the stream was determined by a GC with a FID (TP-2060F), while the CO_2 was analyzed by a GC with a TCD (SP-3420).

The specific activity based on per unit surface area ($-r$) was calculated according to:

$$-r = \frac{F_{\text{acetone,in}} - F_{\text{acetone,out}}}{S_{\text{BET}} W_{\text{cat}}} = \frac{X_{\text{acetone}}}{S_{\text{BET}} W_{\text{cat}} / F_{\text{acetone,in}}}$$

where $F_{\text{acetone,in}}$ and $F_{\text{acetone,out}}$ are molar flow rates of acetone at the inlet and outlet respectively, S_{BET} is the BET surface area of the catalyst, W_{cat} is the catalyst weight, and X_{acetone} is the acetone conversion at a given temperature. The acetone conversion (X_{acetone}) used in the calculation of the specific activity was measured by monitoring the acetone conversion with time-on-stream at 160 °C until stationary value was obtained.

3. Results and discussion

3.1. TG–DSC analysis of the precursor

Fig. 1 shows the TG–DSC curves of the dried $Cu_{0.13}Ce_{0.87}O_y$ precursor obtained from the SCD process. The TG curve in Fig. 1 shows one apparent weight increment and two weight loss steps in the temperature range from 30 to 350 °C. The weight increase about 6.7 wt.% below 50 °C may be attributed to the oxidation of certain amounts of Ce^{3+} in the precursor, which is reflected by an exothermic peak at 42 °C in the DSC profile. The weight loss between 50 and 350 °C was about 21.3 wt.% with regard to the total weight of the catalyst precursor, accompanied by a strong exothermic peak at

Table 1
Average crystallite size, lattice constant, BET surface area, and pore volume of the $Cu_{0.13}Ce_{0.87}O_y$ samples calcined at different temperatures.

Calcination temperature (°C)	Crystallite size (nm)	Lattice constant (nm)	Surface area (m^2/g)	Pore volume (cm^3/g)
400	4.8	0.5391	98.2	0.67
600	7.3	0.5392	87.3	0.55
700	8.4	0.5397	71.1	0.50
800	25.5	0.5400	16.3	0.07

232 °C, which can be primarily attributed to desorption and combustion of ethanol in the precursor. The thermal analysis results indicate that the possible carbon species in the precursor can be removed after calcination at 400 °C in air. Interestingly, a strong endothermic peak at 675 °C was observed in the DSC curve. The previous reported CuO–CeO_2 catalyst precursor prepared by a sol–gel or a co-precipitation method did not show this endothermic peak in the TG–DSC/DTA curves [20,21]. This indicates that the thermal behavior of the catalyst precursor is greatly related to the preparation method. The presence of the endothermic peak at 675 °C may be an indication of a structural change of the sample in this temperature range. The XPS measurement described in later discussion showed that parts of Cu^{2+} were reduced to Cu^+ when increasing the calcination temperature from 600 to 700 °C. Thus, the endothermic peak at 675 °C in the DSC curve was ascribed to the reduction of parts of Cu^{2+} to Cu^+.

3.2. XRD characterization

Fig. 2(a) presents the XRD patterns of the $Cu_{0.13}Ce_{0.87}O_y$ samples calcined at different temperatures. For comparison, the XRD pattern of pure CeO_2 prepared by the present method and calcined at 400 °C is also shown in Fig. 2(a). The typical diffraction peaks of CeO_2 could be seen in all the samples. The diffraction peaks of the $Cu_{0.13}Ce_{0.87}O_y$ samples became sharper with increase in the calcination temperature due to the better crystallization of CeO_2. No peaks corresponding to CuO could be identified for the samples with the calcination temperature up to 700 °C. After calcined at 800 °C for 4 h, the sample showed two very small diffraction peaks of CuO, indicating the formation of bulk CuO in the sample at this calcination temperature. The average crystallite sizes of all the samples calculated according to the Scherrer equation are shown in Table 1. As expected, an increase in the crystallite size was observed for the samples with increasing the calcination temperature from 400 to 800 °C.

Compared to XRD pattern of the pure CeO_2, the diffraction peaks of the $Cu_{0.13}Ce_{0.87}O_y$ samples shifted to higher angles (Fig. 2(b)). The lattice constants of the samples were further calculated for comparison and the results are also listed in Table 1. It can be seen that the calculated lattice constants of all the samples were much lower than that of pure CeO_2 (0.5423 nm), indicating at least parts of copper species were incorporated into the CeO_2 lattice since the radius of Cu^{2+} (0.072 nm) is smaller than that of Ce^{4+} (0.092 nm). The partial substitution of Ce^{4+} by Cu^{2+} would lead to the shrinkage of the CeO_2 lattice, and thus decrease the lattice constant. Compare with our previous reported sample [14], the present catalysts had smaller lattice constants, indicating more copper species were incorporated into the CeO_2 lattice and thus more amounts of oxygen vacancies were formed in the catalyst. Obviously, the decrease in the lattice constant of the sample with the same composition results from the different preparation method, which has effect on the structural characteristics of the final product, such as crystallite size and homogeneity of the constituents.

It should be noted that the XRD patterns of the three samples calcined from 600 to 800 °C displayed a slight shift in the CeO_2 diffraction peaks to low 2θ values (Fig. 2(b)), which can be taken as an indication of lattice expansion. The lattice constants of CeO_2 also increased from 0.5392 to 0.5400 nm for the samples calcined in this temperature range. The increase in the lattice constants of the samples may be related to many factors, such as reduction of Cu^{2+} in the CeO_2 lattice and segregation of copper species from the CeO_2 lattice. Combined with the results of XRD, Raman, and XPS discussed later, it is believed that the increase in the lattice constants of the samples calcined from 600 to 700 °C was due to the fact that parts of Cu^{2+} incorporated into CeO_2 lattice was reduced

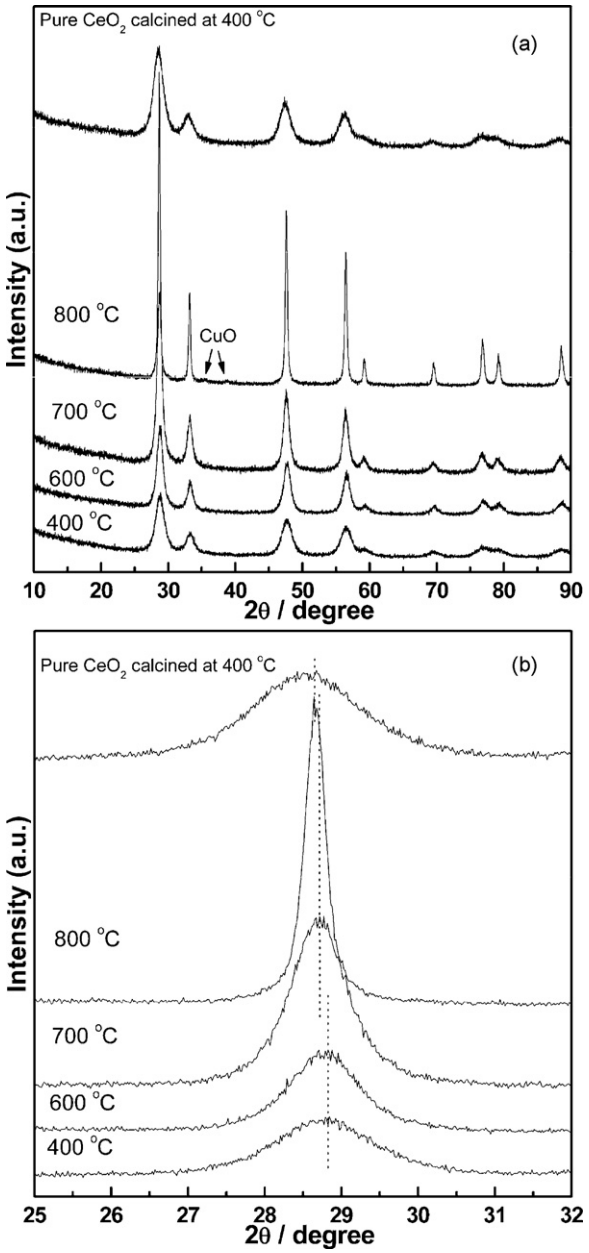

Fig. 2. (a) XRD patterns of pure CeO_2 calcined at 400 °C and the $Cu_{0.13}Ce_{0.87}O_y$ catalysts calcined at different temperatures and (b) enlarged XRD patterns from 2θ range from 25° to 32°.

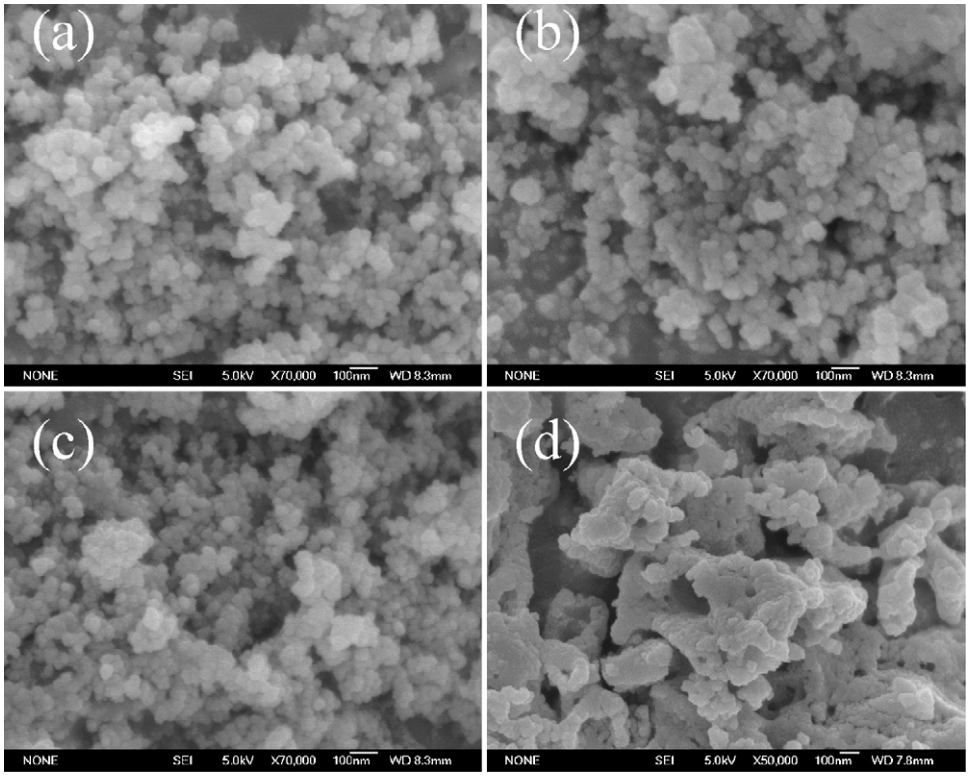

Fig. 3. SEM images of the $Cu_{0.13}Ce_{0.87}O_y$ catalysts calcined at different temperatures: (a) 400 °C, (b) 600 °C, (c) 700 °C, and (d) 800 °C.

to Cu^+ since the radius of Cu^+ (0.096 nm) is larger than that of Cu^{2+}, while the second increase in the lattice constant from 700 to 800 °C was mainly ascribed to the segregation of copper species from the Cu–Ce–O solid solution.

3.3. SEM characterization and BET surface area

The particle sizes and the structure of the catalysts calcined at different temperatures were further investigated by SEM. As shown in Fig. 3, the samples calcined below 800 °C consisted of nanocrystals with average diameters less than 100 nm. After calcined at 800 °C, the particles became larger (Fig. 3(d)), indicating the occurrence of sintering. The particle sizes observed from the SEM image were larger than the crystallite sizes calculated from the XRD pattern, suggesting the powder particles were agglomerated to some extent. The surface area and pore volume of the $Cu_{0.13}Ce_{0.87}O_y$ samples calcined at different temperatures are listed in Table 1. It can be seen that there is a continuous decrease in the BET surface area with increasing the calcination temperature and the decrease is greater after calcination at 800 °C. The dependence of the pore volume on the calcination temperature is consistent with that of the BET surface area. The subsequent decline in the surface area upon thermal treatment at higher temperatures could be due to various factors, such as growth of crystallite size, formation of various mixed oxide phases, and sintering.

3.4. Raman analysis

Fig. 4 shows the Raman spectra of the $Cu_{0.13}Ce_{0.87}O_y$ samples calcined at different temperatures. Three adsorption bands at approximately 462, 600 and 1122 cm^{-1} were observed for all the samples. It is well known that the adsorption peak at 462 cm^{-1} is ascribed to the Raman active F_{2g} mode of CeO_2 cubic lattice, which can be viewed as a symmetric breathing mode of the oxygen atoms around cerium ions [22]. The weak and broad band observed near 600 cm^{-1} and the second-order peak at 1122 cm^{-1} are linked to oxygen vacancies, which usually results from the replacement of Ce^{4+} by metal ion with different valence and forms according to the vacancy compensation mechanism [23–25]. This result further confirmed that at least parts of copper species were truly incorporated into the CeO_2 lattice and formed Cu–Ce–O solid solution, in agreement with the above XRD results. The formation of oxygen vacancies would increase the mobility of lattice oxygen, and consequently the catalytic performance may be favored.

With increasing the calcination temperature from 400 to 800 °C, the band at 462 cm^{-1} became sharpened and more symmetrical. This could be due to the better crystallization of CeO_2 with increase in the calcination temperature. It should be noted that no obvi-

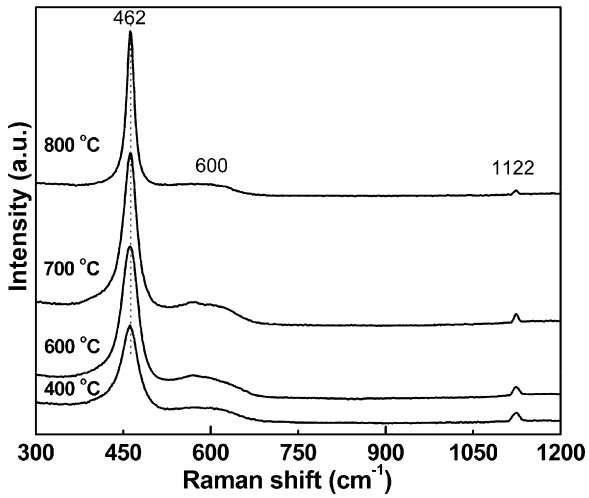

Fig. 4. Raman spectra of the $Cu_{0.13}Ce_{0.87}O_y$ catalysts calcined at different temperatures.

ous shift of the band at 462 cm^{-1} was detected for all the samples. However, the change in the lattice constant, as well as the particle size of CeO_2, should lead to a shift of this band in the Raman spectrum. Spanier et al. observed the peak shift of about 10 cm^{-1} for the band at 462 cm^{-1} when changing the particle size of CeO_2 from 6 to 5 μm [25]. In the present study, the absence of the shift of the F_{2g} mode may be due to the minor change of the lattice constant, resulting in minor variation of Ce–O bond length. In addition, the presence of oxygen vacancies originated from the formation of Cu–Ce–O solid solution may also stabilize the CeO_2 environment despite the growth of the particle size [24].

The intensity of the band at 600 cm^{-1} slightly increased with the calcination temperature from 400 to 700 °C and then decreased after calcined at 800 °C, while the vibration of the band at 1122 cm^{-1} weakened with increasing the calcination temperature. The intensity ratio (I_{600}/I_{462}) of the band at about 600 and 462 cm^{-1} can be used to estimate the oxygen vacancy concentration in the CeO_2 lattice [26]. A rough estimate of the I_{600}/I_{462} showed that the intensity ratio decreased very slightly with increasing the calcination temperature from 400 to 700 °C and then decreased sharply after calcined at 800 °C, suggesting the decrease of oxygen vacancy concentration in the sample. It appears that the tendency of the band at about 600 cm^{-1} is related to the oxygen vacancy concentration and the intensity of the band at 462 cm^{-1}. However, it is difficult to exactly quantify the I_{600}/I_{462} values due to the broad nature of the band. Thus, further analysis of the band at 600 cm^{-1} was not performed in the present study. In the case of the band at 1122 cm^{-1}, the band intensity is considered to be related to the resonance Raman effect [24], which may be related to the crystallite size of CeO_2. Actually, Pu et al. did not observe this band in the Raman spectrum of $Ce_{0.9}Pr_{0.1}O_{2-\delta}$ solid solution with a crystallite size of about 35 nm using an excitation wavelength of 514 nm [27]. The decrease in the band at 1122 cm^{-1} should be due to the increase of CeO_2 crystallite size with increasing the calcination temperature of the sample.

No bands corresponding to CuO were observed in the Raman spectra for all the samples. The usual interpretation for this phenomenon is that CuO is well dispersed in the support structure, and thus cannot be detected by Raman technique. However, the previous XRD pattern of the sample calcined at 800 °C clearly exhibited two weak diffraction peaks of CuO. Two B_g phonon modes located at 330 and 632 cm^{-1} of CuO [28] should appear in the Raman spectrum of the sample calcined at 800 °C. There seems to be a contradiction between the Raman and the XRD results. Shan et al. observed that the Raman bands of CuO could not be clearly distinguished even by the direct physical mixture of CeO_2 and CuO [24]. Instead, the sample showed a reduced Raman mode compared with pure CeO_2 due to the strong adsorption of CuO in the region. In the present study, similar phenomenon was also observed between the samples calcined at 700 and 800 °C. The intensity of the band at 462 cm^{-1} for the two samples decreased slightly with increasing the calcination temperature from 700 to 800 °C, which should be related to the presence of bulk CuO in the sample calcined at 800 °C. Thus, it may be concluded that the absence of CuO bands in the Raman spectrum may be due to its too strong adsorption to be detected or too weak Raman modes that may be overlapped by that of CeO_2. The present results also indicate that the Raman technique is a powerful tool to elucidate the oxygen vacancy, while fails to directly distinguish the dispersion of CuO in CuO–CeO_2 binary system.

3.5. XPS analysis

XPS was further conducted to examine the chemical state of copper and cerium in the samples calcined at different temperatures. As shown in Fig. 5(a), the spectra of Cu $2p_{3/2}$ in all the samples

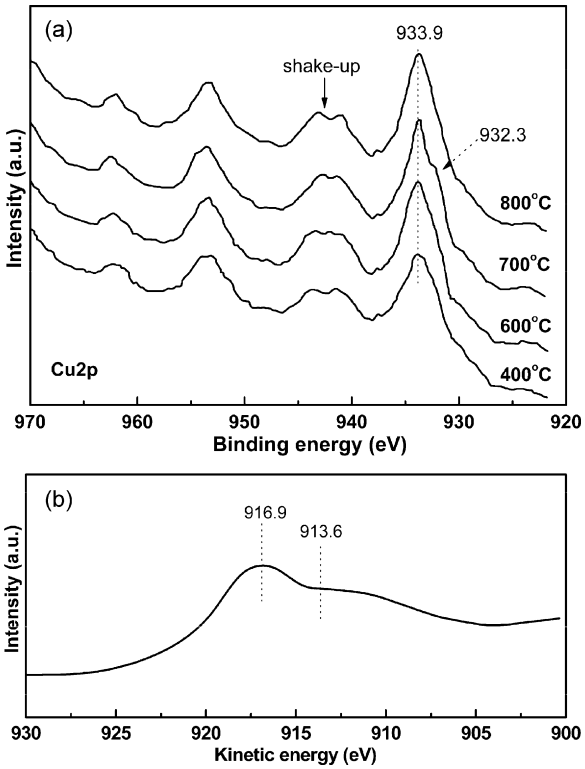

Fig. 5. (a) Cu 2p XPS of the $Cu_{0.13}Ce_{0.87}O_y$ catalysts calcined at different temperatures; (b) kinetic energy spectrum of the Auger L_3VV electron of the sample calcined at 700 °C.

contained an obvious shake-up peak at 939–944 eV and one main peak at 933.9 eV, which are two important XPS characteristics of Cu^{2+}. In addition, the Cu $2p_{3/2}$ spectrum of the sample calcined at 700 °C exhibited a small shoulder peak at about 932.3 eV, which is the characteristic of the reduced copper species [29]. Since the binding energies of Cu^+ and Cu^0 are almost identical [29], the exact judgment of the two copper species should be made according to the Cu–Auger spectrum. Fig. 5(b) shows the kinetic energy spectrum of the Auger L_3VV electron of the sample calcined at 700 °C. The doublet peaks for the kinetic energy spectra of the Auger L_3VV electron indicated the presence of two copper species: the peak at 916.9 eV could be ascribed to Cu^{2+} species and the other peak at 913.6 eV could be assigned to the Cu^+ species. Therefore, the copper atom existed in the form of Cu^{2+} and Cu^+ for the sample calcined at 700 °C, while only Cu^{2+} were presented in the other samples. The Ce 3d region of the samples calcined at different temperatures showed a typical CeO_2 spectrum with two main peaks at 916.7 and 882.3 eV (not shown) [29]. There is no evidence of the presence of Ce in lower oxidation states. XPS results indicated that parts of Cu^{2+} species in the sample underwent a reduction from +2 to +1 with increasing the calcination temperature from 600 to 700 °C, which may be responsible for the endothermic peak at about 675 °C in the DSC curve (Fig. 1) and the shift of 2θ in the XRD patterns for the sample calcined from 600 to 700 °C (Fig. 2(b)).

The co-existence of Cu^{2+} and Cu^+ species in CuO–CeO_2 catalysts has also been observed by other investigators [30–36]. Avgouropoulos et al. [31,32] and Martínez-Arias et al. [33] considered that the presence of reduced states (either Cu^+ or Ce^{3+}) in the CuO–CeO_2 catalyst was greatly related to the pretreatment done on the catalysts or the preparation method of the catalyst. Liu and Flytzani-Stephanopoulos [34] proposed that the reducibility of Ce^{4+} to Ce^{3+} made copper ions incorporated into CeO_2 lattice adapt to a different oxidation state while maintaining the electronic neutrality of the lattice. Hočevar et al. [35] proposed that the for-

Table 2
H_2 uptake of the $Cu_{0.13}Ce_{0.87}O_y$ samples calcined at different temperatures.

Calcination temperature (°C)	Cu/(Cu + Ce) (mol%)[a]	H_2 consumption (mmol/g_{cata})[b]		
		Peak α	Peak β	Total
400	23	0.59	0.85	1.44
600	30	0.55	0.81	1.36
700	31	0.50	0.80	1.30
800	32	–	–	0.87

[a] The nominal value of Cu/(Cu + Ce) molar ratio is 13%.
[b] The nominal value of H_2 uptake is 0.81 mmol/g_{cata}.

mation of Cu^+ might be induced by substitution at the interface of the two oxide phases due to the similarity of Ce^{4+} and Cu^+ ionic radii. Combined with these references and the present XPS results, it appears that the reduction of Cu^{2+} to Cu^+ is due to the more size-compatibility of Cu^+ in the CeO_2 lattice since Cu–Ce–O solid solution formed and no Ce^{3+} presented in the samples. Naturally another question is put forward: why Cu^+ did not exist in the samples calcined at other temperatures. Although the exact reason is not clear, the analysis of the effect of the calcination temperature on the structures of the samples may shed light on understanding this phenomenon. In the present study, various characterization techniques showed that the calcination temperature mainly had effect on the crystallite sizes and redox properties of the samples. Specifically, with increasing the calcination temperature from 400 to 700 °C, the crystallite size of the sample increased gradually and the interaction between CuO and CeO_2 became weaker, as discussed in the following TPR measurement. Based on these results, it is reasonable to suggest that the presence of the Cu^+ species in the CuO–CeO_2 results from not only the size-compatibility of the Ce^{4+} and Cu^+ due to the formation of Cu–Ce–O solid solution, but a moderate interaction between the copper species and cerium oxide probably being related to the crystallite size of the sample.

The surface composition calculated based on the XPS spectra, expressed as Cu/(Cu + Ce) molar ratio, is listed in Table 2. In all cases, the surface Cu/(Cu + Ce) ratio is higher than the nominal value. Furthermore, the Cu/(Cu + Ce) ratio increased with increase in the calcination temperature from 400 to 800 °C. The copper species enrichment on the Cu–Ce–O catalyst surface has also been reported by other investigators [32]. This phenomenon should be related to the lower surface energies of copper species than that of Ce^{4+}. The copper species predominately located on the catalyst surface, and the migration of copper species to the surface, are favorable for reducing the surface energy of Cu–Ce–O binary system.

3.6. Redox properties

The TPR profiles of the $Cu_{0.13}Ce_{0.87}O_y$ samples treated at different calcination temperatures are shown in Fig. 6. For the samples calcined from 400 to 700 °C, two reduction peaks (α and β) in the range of 150–300 °C were clearly observed. In contrast, the TPR profile of the sample calcined at 800 °C exhibited a broad reduction peak with a small shoulder γ at about 260 °C. The reduction features of the samples in the present study seemed to be similar to that of the previous reported results [14].

To further understand the redox behaviors of the samples, the quantitative analysis of the reduction peaks was carried out and the results are shown in Table 2. The amount of consumed hydrogen of all the samples was larger than the one corresponding to the reduction of CuO to Cu, indicating the reduction of CeO_2 also took place alongside with the CuO reduction. The H_2 consumption of the peak α and the peak β, as well as the total H_2 consumption, decreased with increase in the calcination temperature, which had a similar trend to the crystallite sizes of the samples. If the peak α only corresponds to the reduction of finely dispersed CuO, the trend of the consumed H_2 for the peak α should be contrary to that of the experimental values since the Cu/(Cu + Ce) molar ratio increased with increasing the calcination temperature from 400 to 700 °C. Thus, it is highly possible that the low-temperature peak α was due to the reduction of surface oxygen species and the high-temperature peak β was ascribed to the reduction of bulk oxygen in the $Cu_{0.13}Ce_{0.87}O_y$ binary system. In addition, it should be noted that the initial reduction (peak α) may not be confined to the surface but extended deep into the bulk due to the formation of Cu–Ce–O solid solution.

Interestingly, an increased redox behavior was observed for the $Cu_{0.13}Ce_{0.87}O_y$ samples with increasing the calcination temperature from 400 to 700 °C. Similar phenomenon was also observed for CuO–CeO_2 catalysts prepared by a co-precipitation method [21]. Generally, the reduction temperature is greatly related to the structural properties of the catalyst, such as chemical composition, BET surface area, morphology, and particle size. Higher BET surface area and smaller particle size would favor the accessibility of H_2 and reduction of the sample by H_2. It is expected that the reducibility should decrease with increase in the calcination temperature of the sample due to the growth of crystallite size and loss of surface area. Avgouropoulos et al. took the reduction temperature of CuO–CeO_2 system as an indicator of the interaction strength between Cu^{2+} and Ce^{4+}: a lower reduction temperature could be seen as a stronger interaction [32]. Indeed, the reduction behavior of mixed oxides at nanoscale is usually different from that of the sample with large particles due to the occurrence of a more intimate synergism effect.

A comprehensive review on the redox behaviors of mixed oxides may shed light on the understanding the increased redox properties of the samples in the present study. Sagar et al. [37] and Kundakovic and Flytzani-Stephanopoulos [38] showed that copper species, which presented as highly dispersed clusters or as isolated Cu ions strongly interacting with the support, required higher temperature to be reduced than that on the surface with a moderate

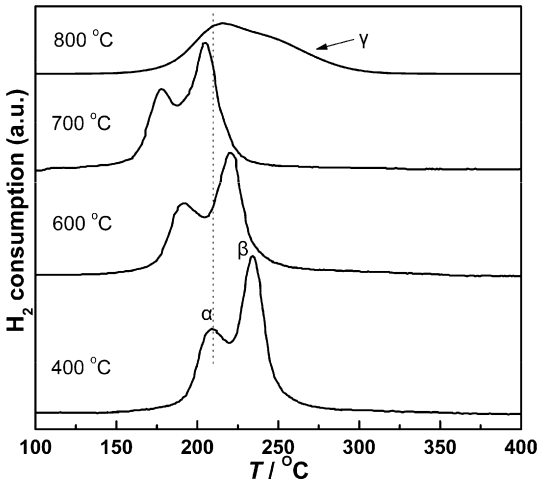

Fig. 6. TPR profiles of the $Cu_{0.13}Ce_{0.87}O_y$ catalysts calcined at different temperatures.

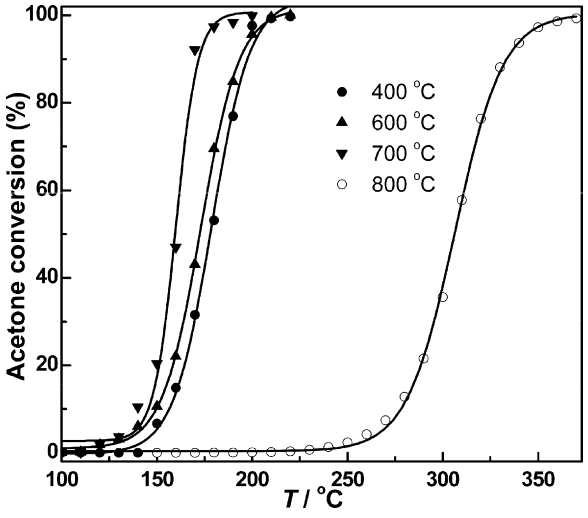

Fig. 7. Ignition curves of acetone over the $Cu_{0.13}Ce_{0.87}O_y$ catalysts calcined at different temperatures, acetone concentration = 1000 ppm, GHSV = 15 000 h^{-1}.

CuO loading. The reducibility of supported cobalt oxide was also found to be greatly related to the particle sizes. An enhanced redox property of supported cobalt oxide from small to larger particles was evidenced by some investigators [39,40]. Based on the above review, it can be proposed that the interaction between mixed oxides may be greatly related to their crystallite or particle sizes. Too small crystallite size of mixed oxide sample may result in too strong interaction of the oxide phases, and thus bring about negative effect on its reducibility. In the present study, the crystallite size of CeO_2 gradually increased and thus the interaction between CuO and CeO_2 became weaker with increase in the calcination temperature from 400 to 700 °C. Therefore, the reducibility of the CuO on the catalyst surface was enhanced and the reduction temperature of CuO on the catalyst surface decreased.

3.7. Catalytic performance and structure–activity relationship

Fig. 7 shows the ignition curves of acetone over the $Cu_{0.13}Ce_{0.87}O_y$ catalysts calcined at different temperatures. Obviously, the acetone conversion increased with increasing the reaction temperature for all the catalysts. Under the investigated conditions, CO_2 and H_2O were the only reaction products detected. No product of selective oxidation is observed for all the catalysts. The carbon mass balances for acetone combustion over these catalysts were in the range of 100 ± 5%. As shown in Fig. 7, the $Cu_{0.13}Ce_{0.87}O_y$ catalyst calcined at 800 °C exhibited a relatively lower catalytic performance for acetone combustion than the other samples, which might be due to its relatively lower surface area and poorer CuO dispersion in the sample. The $Cu_{0.13}Ce_{0.87}O_y$ catalyst calcined at 700 °C showed the highest activity for acetone combustion and the complete conversion of acetone was achieved at 200 °C. It should be noted that an increased catalytic activity was observed for the samples calcined from 400 to 700 °C, which had a similar trend to the reducibility of the samples. Our previous studies and other investigators have proven that acetone combustion over the $Cu_xCe_{1-x}O_y$ catalysts proceeds according to a Mars-van Krevelen mechanism [14,41]. Thus, it is reasonable that the relationship between catalytic activity and reducibility can be established when the catalyst undergoes a redox cycle.

Compared with our previous $Cu_{0.13}Ce_{0.87}O_y$ catalyst prepared by the combustion method, the catalysts in the present study decreased the temperature required for the complete conversion of acetone. However, the direct comparison of the acetone conversion at a given temperature seems unmeaningful due to their

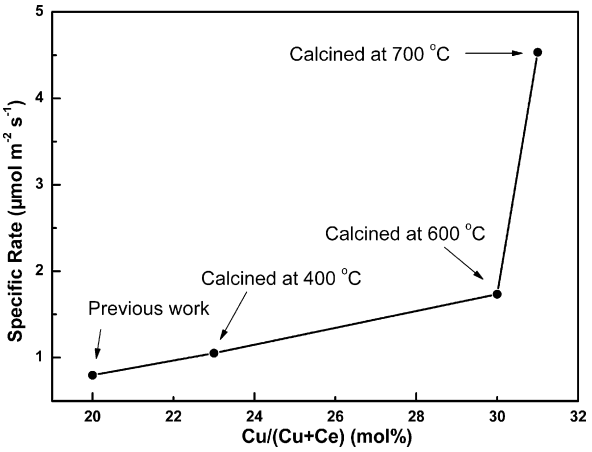

Fig. 8. Specific reaction rate of acetone combustion at 160 °C as a function of Cu/(Cu + Ce) molar ratio on the catalyst surface.

different surface areas. In this case, the comparison of the specific activity based on per unit surface area of the catalyst would be more reasonable [42]. Fig. 8 shows the specific activity of each catalyst for acetone combustion at 160 °C as function of Cu/(Cu + Ce) molar ratio on the catalyst surface. It can be seen that the present catalysts with higher Cu/(Cu + Ce) ratios truly exhibited higher specific activities than the previous catalyst. This result further confirms that the highly dispersed CuO exposed on the catalyst surface is the main active site for the acetone combustion. In addition, it should be noted that the specific activity of the sample calcined at 700 °C increased much greater than the other samples. Taken into account the XPS results, it may be concluded that the presence of Cu^+ on the catalyst surface has a positive effect on the acetone combustion. However, due to the limitation of our techniques, the role of the Cu^+ for acetone combustion is still not clear and needed further study.

3.8. Stability test

A series of long catalytic runs were performed with the reactor operating at a constant temperature to evaluate the catalyst stability. The stability as function of time on stream of the three catalysts at 200 °C is indicated in Fig. 9. During the first 5 h on stream, the catalysts calcined at 600 and 700 °C showed slight decrease in their catalytic activities for acetone combustion, while the catalyst calcined at 400 °C suffered a more noticeable deactivation. After this

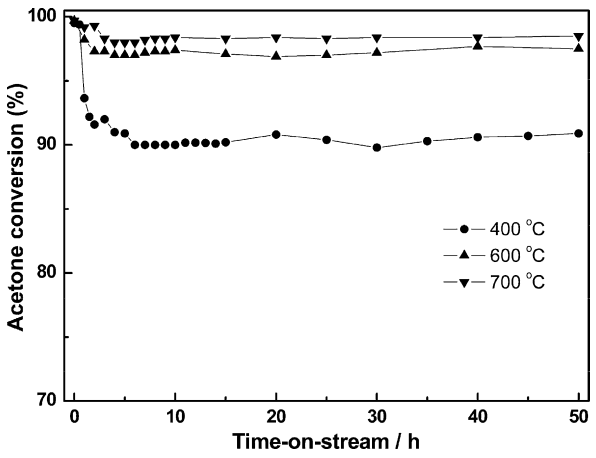

Fig. 9. Evolution of acetone conversion at 200 °C with time-on-stream for the $Cu_{0.13}Ce_{0.87}O_y$ catalysts calcined from 400 to 700 °C, acetone concentration = 1000 ppm, GHSV = 15 000 h^{-1}.

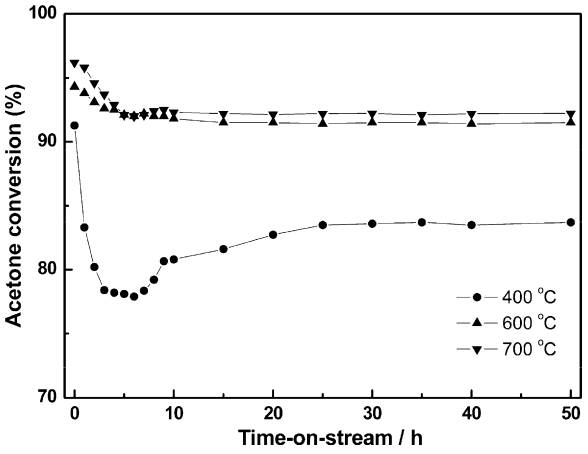

Fig. 10. Evolution of acetone conversion at 300 °C with time-on-stream for the $Cu_{0.13}Ce_{0.87}O_y$ catalysts calcined at different temperatures, acetone concentration = 1000 ppm, GHSV = 90 000 h^{-1}.

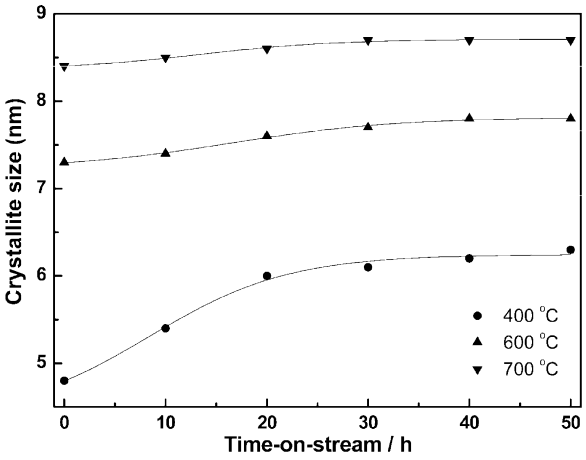

Fig. 11. Crystallite sizes of the catalysts after different time-on-stream at 300 °C.

period, the acetone conversion over the three catalysts remained almost constant in the following 45 h on stream. The presence of an initial transient period before reaching a steady state mainly lies in the fact that time is always needed to get a constant coverage on the catalyst surface by the reactants and the products [43]. The decrease in the acetone conversions over the catalysts may be due to the adsorption of water on the active sites of the catalyst [44]. It should be noted that the extent of the decrease in acetone conversion for the catalyst calcined at 400 °C was greater than that of the other two samples. It appears that the above reason is not the only one for the observed activity loss of the catalyst calcined at 400 °C. Another factor that must be considered for catalyst is the surface area. Thus, the surface areas of the three catalysts after used for 50 h were determined. The results showed that the degree in the loss of the surface areas differed from catalyst to catalyst under the same conditions and was of the following order: the catalyst calcined 400 °C (7.4%) > 600 °C (2.0%) > 700 °C (1.1%). Therefore, the loss of surface area of the catalysts may also contribute to the decrease in catalytic activity, especially of the catalyst calcined at 400 °C.

The catalyst stability was further evaluated by conducting endurance test at higher temperature and GHSV. The evolution of acetone conversion with time-on-stream at 300 °C is presented in Fig. 10. It should be noted that direct comparison of Figs. 9 and 10 is difficult due to the different reaction temperature and GHSV used in the tests. As shown in Fig. 10, the catalysts calcined at 600 and 700 °C showed slight decrease in the acetone conversion at the initial stage, being similar to the endurance behaviors observed at 200 °C. Interestingly, the evolution of acetone conversion with time on stream over the catalyst calcined at 400 °C was different from that of the other two catalysts. The acetone conversion decreased for the first 6 h, then gradually increased to a higher value, and finally sustained at a constant in the following time on stream. The changes observed in the performance suggested that the catalyst calcined at 400 °C experienced structural change with time on stream.

As discussed earlier, the catalytic activity of the $Cu_{0.13}Ce_{0.87}O_y$ catalyst for acetone combustion is greatly related to its reducibility that may be related to the crystallite size of the catalyst. In order to understand this behavior of the catalyst, XRD and TPR were used to characterize the used catalyst with different time on stream. For comparison, the other two catalysts were also characterized. XRD results showed that the crystallite size of the catalyst calcined at 400 °C gradually increased from 4.8 to 6.3 nm with time on stream at 300 °C, while the other two catalysts remained almost unchanged (Fig. 11). TPR result (not shown) revealed an enhanced reducibility of the used catalyst than the fresh one calcined at 400 °C. Thus, the change in the stability of the catalyst calcined at 400 °C can be explained as follows: during the first 5 h on stream, the loss of surface area and the adsorption of water on the active sites may be responsible for the decrease in catalytic activity until a transitional steady state was reached. Simultaneously, the crystallite size of the sample increased with time on stream under the present experimental conditions. It led to a relatively weak interaction between CuO and CeO_2 and an enhanced redox property, which resulted in the improvement of its catalytic activity for acetone combustion. Following this transition period, the formation of larger steady state crystallite size of the catalyst was completed and a stable catalytic activity was established.

4. Conclusions

In summary, $Cu_{0.13}Ce_{0.87}O_y$ catalysts with enhanced catalytic activity and stability compared to our previous reported sample were prepared by a supercritical drying technique and calcination steps. The structural characteristics of the as-prepared nanocrystalline $Cu_{0.13}Ce_{0.87}O_y$ catalyst were found to be strongly depended on the calcination temperature. The XRD and Raman results indicated the $Cu_{0.13}Ce_{0.87}O_y$ catalysts calcined from 400 to 800 °C were in the form of Cu–Ce–O solid solution, while the XPS measurements showed that the copper species were predominately located on the surface of the CeO_2 nanocrystalline aggregates. The redox properties and the catalytic activities for acetone combustion of the catalysts were also related to the calcination temperature and their crystallite sizes. Too small crystallite size may bring about negative influence on the redox property, which then affects the catalytic activity of the catalyst. The $Cu_{0.13}Ce_{0.87}O_y$ catalyst calcined at 700 °C, which could convert acetone completely into CO_2 and H_2O at 200 °C, was the most active catalyst. Stability tests of the $Cu_{0.13}Ce_{0.87}O_y$ catalysts calcined from 400 to 700 °C suggested that catalysts lost some activity in the initial time on stream but were stabilized thereafter. The decrease in the catalytic activities of the catalysts for acetone combustion may be due to the loss of the surface area and adsorption of water on the active sites. In addition, the presence of Cu^+ on the catalyst surface seems to have positive effect on acetone combustion. Further study is still needed to clarify the exact role of Cu^+ by using other characterization techniques, such as in situ FTIR.

References

[1] N. Burgos, M. Paulis, M.M. Antxustegi, M. Montes, Deep oxidation of VOC mixtures with platinum supported on Al_2O_3/Al monoliths, Appl. Catal. B: Environ. 38 (2002) 251–258.

[2] A. Gil, M.A. Vicente, J.-F. Lambert, L.M. Gandía, Platinum catalysts supported on Al-pillared clays application to the catalytic combustion of acetone and methyl-ethyl-ketone, Catal. Today 68 (2001) 41–51.
[3] M. Paulis, L.M. Gandía, A. Gil, J. Sambeth, J.A. Odriozola, M. Montes, Influence of the surface adsorption–desorption processes on the ignition curves of volatile organic compounds (VOCs) complete oxidation over supported catalysts, Appl. Catal. B: Environ. 26 (2000) 37–46.
[4] L.M. Gandía, A. Gil, S.A. Korili, Effects of various alkali–acid additives on the activity of a manganese oxide in the catalytic combustion of ketones, Appl. Catal. B: Environ. 33 (2001) 1–8.
[5] V. Blasin-Aubé, J. Belkouch, L. Monceaux, General study of catalytic oxidation of various VOCs over $La_{0.8}Sr_{0.2}MnO_{3+x}$ perovskite catalyst-influence of mixture, Appl. Catal. B: Environ. 43 (2003) 175–186.
[6] T.S.C. Law, C. Chao, G.Y.W. Chan, A.K.Y. Law, Confined catalytic oxidation of volatile organic compounds by transition metal containing zeolites and ionizer, Atmos. Environ. 37 (2003) 5433–5437.
[7] R. Spinicci, M. Faticanti, P. Marini, S. De Rossi, P. Porta, Catalytic activity of $LaMnO_3$ and $LaCoO_3$ perovskites towards VOCs combustion, J. Mol. Catal. A: Chem. 197 (2003) 147–155.
[8] D.P. Das, K.M. Parida, Mn(III) oxide pillared titanium phosphate (TiP) for catalytic deep oxidation of VOCs, Appl. Catal. A: Gen. 324 (2007) 1–8.
[9] D. Frías, S. Nousir, I. Barrio, M. Montes, T. López, M.A. Centeno, J.A. Odriozola, Synthesis and characterization of cryptomelane- and birnessite-type oxides: precursor effect, Mater. Charact. 58 (2007) 776–781.
[10] T. Mishra, P. Mohapatra, K.M. Parida, Synthesis, characterisation and catalytic evaluation of iron–manganese mixed oxide pillared clay for VOC decomposition reaction, Appl. Catal. B: Environ. 79 (2008) 279–285.
[11] P.-O. Larsson, A. Andersson, Oxides of copper, ceria promoted copper, manganese and copper manganese on Al_2O_3 for the combustion of CO, ethyl acetate and ethanol, Appl. Catal. B: Environ. 24 (2000) 175–192.
[12] A. Martínez-Arias, M. Fernández-García, J. Soria, J.C. Conesa, Spectroscopic study of a Cu/CeO_2 catalyst subjected to redox treatments in carbon monoxide and oxygen, J. Catal. 182 (1999) 367–377.
[13] G. Qi, R.T. Yang, Performance and kinetics study for low-temperature SCR of NO with NH_3 over MnO_x–CeO_2 catalyst, J. Catal. 217 (2003) 434–441.
[14] C. Hu, Q. Zhu, Z. Jiang, L. Chen, R. Wu, Catalytic combustion of dilute acetone over Cu-doped ceria catalysts, Chem. Eng. J. 152 (2009) 583–590.
[15] G. Marbán, I. López, T. Valdés-Solís, Preferential oxidation of CO by CuO_x/CeO_2 nanocatalysts prepared by SACOP. Mechanisms of deactivation under the reactant stream, Appl. Catal. A: Gen. 361 (2009) 160–169.
[16] X. Qi, M. Flytzani-Stephanopoulos, Activity and stability of Cu–CeO_2 catalysts in high-temperature water–gas shift for fuel-cell applications, Ind. Eng. Chem. Res. 43 (2003) 3055–3062.
[17] B. Wen, M. He, Study of the Cu–Ce synergism for NO reduction with CO in the presence of O_2, H_2O and SO_2 in FCC operation, Appl. Catal. B: Environ. 37 (2002) 75–82.
[18] H.Y. Wang, E. Ruckenstein, Partial oxidation of methane to synthesis gas over alkaline earth metal oxide supported cobalt catalysts, J. Catal. 199 (2001) 309–317.
[19] A. Baylet, S. Royer, P. Marécot, J.M. Tatibouët, D. Duprez, High catalytic activity and stability of Pd doped hexaaluminate catalysts for the CH_4 catalytic combustion, Appl. Catal. B: Environ. 77 (2008) 237–247.
[20] M.-F. Luo, Y.-P. Song, X.-Y. Wang, G.-Q. Xie, Z.-Y. Pu, P. Fang, Y.-L. Xie, Preparation and characterization of nanostructured $Ce_{0.9}Cu_{0.1}O_{2-\delta}$ solid solution with high surface area and its application for low temperature CO oxidation, Catal. Commun. 8 (2007) 834–838.
[21] C.R. Jung, J. Han, S.W. Nam, T.-H. Lim, S.-A. Hong, H.-I. Lee, Selective oxidation of CO over CuO–CeO_2 catalyst: effect of calcination temperature, Catal. Today 93–95 (2004) 183–190.
[22] B.M. Reddy, A. Khan, Y. Yamada, T. Kobayashi, S. Loridant, J.-C. Volta, Raman and X-ray photoelectron spectroscopy study of CeO_2–ZrO_2 and V_2O_5/CeO_2–ZrO_2 catalysts, Langmuir 19 (2003) 3025–3030.
[23] J.R. Mcbride, K.C. Hass, B.D. Poindexter, W.H. Weber, Raman and X-ray studies of $Ce_{1-x}Re_xO_{2-y}$, where Re = La, Pr, Nd, Eu, Gd, and Tb, J. Appl. Phys. 76 (1994) 2435–2441.
[24] W. Shan, W. Shen, C. Li, Structural characteristics and redox behaviors of $Ce_{1-x}Cu_xO_y$ solid solutions, Chem. Mater. 15 (2003) 4761–4767.
[25] J.E. Spanier, R.D. Robinson, F. Zhang, S.-W. Chan, I.P. Herman, Size-dependent properties of CeO_{2-y} nanoparticles as studied by Raman scattering, Phys. Rev. B 64 (2001) 245407–245414.
[26] C. Liang, Z. Ma, H. Lin, L. Ding, J. Qiu, W. Frandsen, D. Su, Template preparation of nanoscale $Ce_xFe_{1-x}O_2$ solid solutions and their catalytic properties for ethanol steam reforming, J. Mater. Chem. 19 (2009) 1417–1424.
[27] Z.-Y. Pu, J.-Q. Lu, M.-F. Luo, Y.-L. Xie, Study of oxygen vacancies in $Ce_{0.9}Pr_{0.1}O_{2-\delta}$ solid solution by in situ X-ray diffraction and in situ Raman spectroscopy, J. Phys. Chem. C 111 (2007) 18695–18702.
[28] K. Reimann, K. Syassen, Pressure dependence of Raman modes in CuO, Solid State Commun. 76 (1990) 137–140.
[29] C.D. Wagner, W.M. Riggs, L.E. Davis, J.F. Moulder, G.E. Muilenberg, Handbook of X-Ray Photoelectron Spectroscopy, Perkin-Elmer Corp., Palo Alto, CA, 1978.
[30] Y.-Z. Chen, B.-J. Liaw, H.-C. Chen, Selective oxidation of CO in excess hydrogen over $CuO/Ce_xZr_{1-x}O_2$ catalysts, Int. J. Hydrogen Energy 31 (2006) 427–435.
[31] G. Avgouropoulos, T. Ioannides, H. Matralis, Influence of the preparation method on the performance of CuO–CeO_2 catalysts for the selective oxidation of CO, Appl. Catal. B: Environ. 56 (2005) 87–93.
[32] G. Avgouropoulos, T. Ioannides, Effect of synthesis parameters on catalytic properties of CuO–CeO_2, Appl. Catal. B: Environ. 67 (2006) 1–11.
[33] A. Martínez-Arias, A.B. Hungría, G. Munuera, D. Gamarra, Preferential oxidation of CO in rich H_2 over CuO/CeO_2: details of selectivity and deactivation under the reactant stream, Appl. Catal. B: Environ. 65 (2006) 207–216.
[34] W. Liu, M. Flytzani-Stephanopoulos, Total oxidation of carbon-monoxide and methane over transition metal fluorite oxide composite catalysts. II. Catalyst characterization and reaction-kinetics, J. Catal. 153 (1995) 317–332.
[35] S. Hočevar, U.O. Krašovec, B. Orel, A.S. Arico, H. Kim, CWO of phenol on two differently prepared CuO–CeO_2 catalysts, Appl. Catal. B: Environ. 28 (2000) 113–125.
[36] E. Moretti, M. Lenarda, L. Storaro, A. Talon, T. Montanari, G. Busca, E. Rodríguez-Castellón, A. Jiménez-López, M. Turco, G. Bagnasco, R. Frattini, One-step synthesis of a structurally organized mesoporous CuO–CeO_2–Al_2O_3 system for the preferential CO oxidation, Appl. Catal. A: Gen. 335 (2008) 46–55.
[37] G.V. Sagar, P.V.R. Rao, C.S. Srikanth, K.V.R. Chary, Dispersion and reactivity of copper catalysts supported on Al_2O_3–ZrO_2, J. Phys. Chem. B 110 (2006) 13881–13888.
[38] L. Kundakovic, M. Flytzani-Stephanopoulos, Reduction characteristics of copper oxide in cerium and zirconium oxide systems, Appl. Catal. A: Gen. 171 (1998) 13–29.
[39] R. Bechara, D. Balloy, J.-Y. Dauphin, J. Grimblot, Influence of the characteristics of γ-aluminas on the dispersion and the reducibility of supported cobalt catalysts, Chem. Mater. 11 (1999) 1703–1711.
[40] A.Y. Khodakov, A. Griboval-Constant, R. Bechara, F. Villain, Pore-size control of cobalt dispersion and reducibility in mesoporous silicas, J. Phys. Chem. B 105 (2001) 9805–9811.
[41] E. Finocchio, R.J. Willey, G. Busca, V. Lorenzelli, FTIR studies on the selective oxidation and combustion of light hydrocarbons at metal oxide surfaces, J. Chem. Soc., Faraday Trans. 93 (1997) 175–180.
[42] D. Delimaris, T. Ioannides, VOC oxidation over CuO–CeO_2 catalysts prepared by a combustion method, Appl. Catal. B: Environ. 89 (2009) 295–302.
[43] C. Lahousse, A. Bernier, P. Grange, B. Delmon, P. Papaefthimiou, T. Ioannides, X. Verykios, Evaluation of γ-MnO_2 as a VOC removal catalyst: comparison with a noble metal catalyst, J. Catal. 178 (1998) 214–225.
[44] K.M. Parida, A. Samal, Catalytic combustion of volatile organic compounds on Indian Ocean manganese nodules, Appl. Catal. A: Gen. 182 (1999) 249–256.